ACS Catalysis

RESEARCH ARTICLE

pubs.acs.org/acscatalysis

Propane Oxidation over $Pt/SrTiO_3$ Nanocuboids

James A. Enterkin,[†,§] Worajit Setthapun,[†] Jeffrey W. Elam,[‡] Steven T. Christensen,[‡] Federico A. Rabuffetti,[§] Laurence D. Marks,[∥] Peter C. Stair,[†,§] Kenneth R. Poeppelmeier,[†,§] and Christopher L. Marshall*[,†]

[†]Chemical Sciences and Engineering Division and [‡]Energy Systems Division, Argonne National Laboratory, Argonne, Illinois 60439, United States

[§]Department of Chemistry and [∥]Department of Materials Science and Engineering, Northwestern University, Evanston, Illinois 60208, United States

ABSTRACT: $Pt/SrTiO_3$ shows promise as a low temperature hydrocarbon combustion catalyst for automotive applications. In this study, $SrTiO_3$ nanocuboid supports were synthesized using sol-precipitation coupled with hydrothermal synthesis, and platinum was deposited on the nanocuboids with 1, 3, and 5 cycles of atomic layer deposition (ALD). The platinum particles have a highly uniform distribution both before and after reaction testing, and range from 1 to 5 nm in size, depending upon the number of ALD cycles. These materials have a >50 °C lower light-off temperature for propane oxidation than a conventional Pt/Al_2O_3 catalyst, turn over frequencies up to 3 orders of magnitude higher, and show improved resistance to deactivation. The increased activity is attributed to the stabilization of a Pt/PtO core/shell structure during operating conditions by the strong epitaxy between the Pt and the $SrTiO_3$ support.

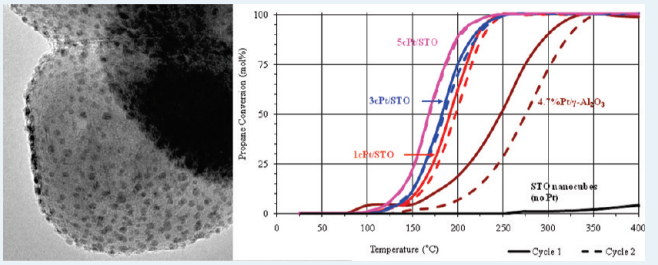

KEYWORDS: platinum, propane oxidation, $SrTiO_3$, atomic layer deposition, nanocrystal support, nanoparticle catalysis

1. INTRODUCTION

Automotive exhaust is one of the main generators of air pollutants. This problem is expected to worsen as the demand for privately owned vehicles increases. Internal combustion engines utilizing gasoline and diesel generate harmful pollutants such as nitrogen oxides (NOx), carbon monoxide (CO), unburned hydrocarbons (HC), particulates, and sulfur oxides (SOx). Liquefied petroleum gas (LPG), an alternative cleaner burning fuel, is gaining ground for use in internal combustion engines.[1] Liquefied petroleum gas has a higher octane rating and produces considerably lower CO, HC, CO_2 and particulate matter emissions compared to gasoline, provided the vehicle is retrofitted for LPG use.[1,2] However, tailpipe emissions from LPG fueled vehicles still contain high concentrations of light alkanes.[3] Up to 80% of the HC emissions are produced in the first 60 to 90 s following a cold-start because of the catalytic converter's inability to oxidize HCs at low temperatures (between 200 to 300 °C).[4] The aim of this work is to develop and characterize low light-off platinum-based HC oxidation catalysts in an effort to reduce tailpipe HC emissions. The study focuses on propane oxidation since propane is the main component in LPG and is found in automotive exhaust.

Platinum is one of the most active materials for HC oxidation. There is some debate in the literature about whether the platinum particle size or shape affects the catalyst activity. While some studies show that the reaction rate per platinum atom does not significantly change with particle size or dispersion, the reaction rate per *surface* platinum atom increases for larger platinum particle sizes.[5−8] Conversely, it has even been observed that nanoscale platinum clusters show entirely different catalytic behavior than larger platinum particles, producing partially oxidized products.[9]

One explanation put forth for the increased activity of larger particles is that metallic platinum may be the active phase, and in an oxidizing environment smaller particles contain more PtO or PtO_2 and less metallic platinum.[8] If such is the case, the challenge would be to maintain platinum in a reduced state with high dispersion under an oxidizing atmosphere. Yoshida and co-workers reported that the total electrophilic and electrophobic properties obtained from the support and additives control the oxidation state of platinum.[10,11] More electrophilic character would result in less oxidized platinum, thus higher catalytic activity.[10−12] Acidic supports and highly electronegative additives promoted Pt stabilization in the metallic phase.[12]

Perovskite-based materials (ABO_3) have been investigated since the 1970s as promising automotive exhaust catalysts to replace the existing noble metal-based catalysts.[13,14] These materials are attractive for deep oxidation because of their surface redox properties, high bulk oxygen mobility, and good thermal stability.[15−17] However, perovskites are generally less active for hydrocarbon oxidation than noble metal catalysts.[15,18] To improve the oxidation activity, noble metals such as Pt and Pd were partially substituted into position B of the $LaMnO_3$-based catalysts.[18,19] However, the activity of volatile organic compound oxidation for such catalysts was similar to the original perovskite.[18] Incipient wetness was used to deposit noble metals on the surface instead of metal substitution

Received: February 18, 2011
Revised: April 26, 2011
Published: April 28, 2011

in the perovskite structure. Impregnating Pd over $LaMnO_3$-based materials produced active catalysts for methane combustion.[19,20] Thus, perovskite supported noble metals showed promise as active hydrocarbon oxidation catalysts. In this work, Pt on strontium titanate, $SrTiO_3$, (STO) nanocuboid supports was studied for propane oxidation.

STO single crystal surfaces have been widely studied as models for mixed-metal oxide catalysts; an extensive array of ultrahigh vacuum surface science techniques has been employed to tailor and characterize their composition and atomic structure.[21,22] Although this approach allows the establishment of surface structure-surface chemistry relationships that are relevant to heterogeneous catalysis, the almost negligible surface area of these flat, nonporous single crystals, render difficult their use in practical catalytic investigations. This problem can be overcome by employing one of the many synthetic approaches that have emerged during the past two decades for the preparation of perovskite oxide nanoparticles with controlled size and shape. These approaches include sol-precipitation,[23−27] hydrothermal synthesis,[26,28] and reverse micelles.[29,30] Owing to their medium-high surface area, nonporosity, and flat surfaces, oxide nanocrystals with highly symmetrical shapes (cubic, octahedral, cuboctahedral, etc.) are attractive as supports for nanosized metal and metal oxide clusters. They may allow the previous knowledge of single crystal surfaces to be applied to the understanding of support surfaces and the interface between catalyst and support. STO nanocrystals with cuboid morphology are of particular interest as a support, as they have the long studied (001) faces primarily exposed.[31] For example, it has recently been shown that the oriented surface of such supports leads to the exposure of different metal catalyst faces than what is normally observed.[32] This allows the formation of stable metal catalyst particles with surface to volume ratios which differ from, and potentially exceed, those found on polycrystalline supports.[32] Additionally, platinum on the STO nanocuboid supports has been seen to be less oxidized than platinum on either alumina or titania supports under similar conditions.[33] Therefore, such supports show potential for increased activity whether the oxidation state of the platinum or the footprint size of the alkane is the primary determinant of activity.

The preparation of *uniform* metallic clusters remains, nonetheless, challenging. Synthetic approaches to this problem have been described by a number of authors,[34] and can be grouped into three main categories: (1) impregnation, (2) ion-exchange, and (3) deposition-precipitation. One-pot synthesis techniques, such as flame synthesis,[35,36] can also create relatively well dispersed and size controlled particles, but have not yet been demonstrated to produce supports of controlled shape. Although these methods are effective in terms of producing catalytically active material, they lack *atomic-level* control over the catalyst composition and surface structure, resulting in inhomogeneous metal clusters, which ultimately imposes a limit on the understanding of their surface chemistry.[34] Thin film growth techniques are attractive as an alternative for depositing metal and metal oxide nanosized clusters on high surface area supports. In particular, atomic layer deposition (ALD) has recently shown great promise in depositing nano sized noble metal clusters.[32,33,37−40] With this technique, highly dispersed and uniform Pt particles are formed on the STO support with a growth rate of ≈0.5 Å per ALD cycle. Although this is in contrast to the typical idealized layered growth of ALD processes, such particle growth is well-known[32−34,37−40] and fits the thermodynamically stable metal morphology.[32]

The ability to tailor catalyst sites is the key to catalyst synthesis. ALD of metal nanoparticles on oxide nanocrystal supports allows precise control of the active metal particle size and distribution. Depositing Pt by ALD over STO nanocuboids resulted in small, uniform sized, well dispersed, crystalline platinum metal particles, which were active as an oxidation catalyst with a lower propane oxidation light-off temperature than the conventional Pt/Al_2O_3 catalyst.

2. EXPERIMENTAL SECTION

2.1. Catalyst Preparation. *2.1.1. $SrTiO_3$ Nanocuboid Synthesis.* $SrTiO_3$ nanocuboids were synthesized following a sol-precipitation—hydrothermal treatment procedure similar to that described in a previous paper.[41] Briefly, ∼80 mL of an aqueous solution containing stoichiometric amounts of Sr and Ti was prepared using $Sr(OH)_2 \cdot 8H_2O$ and $TiCl_4$ as metallic precursors. Coprecipitation of $SrTiO_3$ was induced by adding ∼5 g of NaOH pellets to the above bimetallic precursor solution. Upon dissolution of the NaOH pellets, a highly viscous suspension was obtained, which was subsequently transferred to a 125 mL Teflon-lined autoclave and heated at 240 °C for 36 h. The solution was filtered, and the product washed thoroughly with double-deionized water, and dried at 80 °C for 24 h.

2.1.2. Pt Atomic Layer Deposition. The Pt catalyst was deposited onto the STO nanocuboids using ALD as previously described.[33,37] Briefly, ∼0.25 g of the STO nanocuboids were spread in a stainless steel tray which was covered by a stainless steel mesh to contain the powder while allowing easy access by the ALD precursors[42] and cleaned in situ using a 400 sccm flow of 10% ozone in oxygen at a temperature of 300 °C. The Pt ALD was accomplished using alternating, 200 s exposures to 0.05 Torr (methylcyclopentadienyl) trimethylplatinum ($MeCpPtMe_3$) and 0.20 Torr oxygen at 300 °C[43] using a viscous flow ALD reactor[44] with a constant 90 sccm flow of ultrahigh purity nitrogen (99.995%) carrier gas at a pressure of 0.90 Torr. Nitrogen purge periods of 50 s were used between reactant exposures. A series of Pt catalyst samples were prepared using 1, 2, 3, 4, and 5 Pt ALD cycles over $SrTiO_3$ (1−5cPt/STO). The sample mass was measured using an analytical balance before and after the Pt ALD to determine the Pt loading. A control sample was prepared on commercial STO powder composed of ∼500 nm particles with a specific surface area of 2 m^2/g, using 1c Pt ALD to yield a mass loading of 0.4%. A second control sample was prepared according to the methods of Gluhoi et al.[45]

2.2. Catalyst Characterization. *2.2.1. Electron Microscopy.* Scanning electron microscopy (SEM) images of STO nanocuboids and STO powder were acquired before and after the Pt ALD and also before and after catalytic testing using a Hitachi S4700 with a field emission gun electron beam source operated at 20 kV. Transmission electron microscopy (TEM) and high-resolution electron microscopy (HREM) images of Pt/STO nanocuboids were obtained before and after catalytic testing using a JEOL JEM-2100F electron microscope operated at 200 kV.

2.2.2. Surface Area Measurements. Brunauer−Emmett−Teller (BET) surface areas were measured at −196 °C using a Micromeritics ASAP 2010 analyzer. Samples were degassed overnight at 200 °C under vacuum prior to the measurement.

2.2.3. X-ray Diffraction. X-ray diffraction patterns were collected using a Rigaku DMAX diffractometer in the Bragg−Brentano configuration operated at 20 mA and 40 kV. CuKα radiation (λ = 1.5418 Å) filtered with Ni was employed. The step size and collection time were 0.025° and 1s per step, respectively.

2.2.4. Dispersion Calculations. Platinum dispersion (the percentage of platinum atoms at the surface) was calculated from CO chemisorption data. The sample was reduced in situ in a

Zeton Altamira AMI-100 with 3% H_2 in argon at 300 °C, cooled to −50 °C in argon, and pulsed with CO. CO in the gas output after each pulse was measured by a Dycor Dymaxion quadrupole mass spectrometer. CO adsorption on γ-Al_2O_3 was assumed to be negligible for purposes of calculating Pt dispersion on Pt/γ-Al_2O_3, while CO was assumed to adsorb stoichiometrically to surface Pt atoms. CO adsorption on STO nanocuboids was measured at 2.18 CO atoms adsorbed per nm^2 of STO surface. This was used to correct the Pt dispersion for the Pt/STO nanocuboid catalysts. Using a hemispherical model for the platinum particles (which is not the true particle morphology,[32] but close enough for particle size estimation), we calculated the average Pt particle radius which would expose the proper amounts of platinum and cover the correct amount of support surface to account for the observed CO adsorption.

2.3. Catalytic Testing. The propane oxidation light-off experiments were conducted in a 1/4″ OD fused silica U-tube plug-flow microreactor. The reactor was charged with the catalyst and placed in a clamshell furnace (Applied Test Systems). A K-type thermocouple was then positioned at the top of the catalyst bed. The feed direction is from top to bottom of the catalyst bed. The reactor temperature was controlled using a programmable temperature controller (Eurotherm 2416 series). The reaction products were quantified using a gas chromatograph (HP5820 SeriesII) equipped with Rt-MSieve 5A PLOT and Rt-QPLOT columns. Pt/STO was evaluated for propane oxidation light-off temperature (T_{50}) and propane turnover frequency (TOF). The catalysts were used as prepared, without pretreatment. Light-off temperature, T_{50}, is defined as the temperature at which 50% propane conversion is achieved. The T_{50} were measured at propane weight hourly space velocity (WHSV) of 4 h^{-1} when comparing the different Pt loadings on STO nanocubes and γ-Al_2O_3, and at propane WHSV of 390 h^{-1} when comparing the STO nanocube and the powder STO supports. The WHSV was calculated based on the total amount of C_3H_8 (mol/h) over total mol of Pt on the catalyst. To determine the T_{50}, the C_3H_8 conversion was measured at room temperature with 25 °C increments up to 400 °C. Afterward, the catalyst was cooled down to room temperature in reactant gas. A second temperature ramp was then performed to check for reproducibility. Catalysts which showed no deactivation after a second cycle up to 400 °C (i.e., those on STO supports) were then cycled up to 550 °C to check for deactivation. The reactant mixture for T_{50} measurements consisted of 0.25% C_3H_8 and 3.75% O_2 with Ar as a diluent. Propane oxidation TOFs were measured at 250 °C with the catalyst in the range of 1−60 mg. The propane WHSV were varied (6,000−50,000 h^{-1} for Pt/STO nanocuboids, 100−300 h^{-1} for Pt/STO powder and Pt/γ-Al_2O_3) to limit the propane conversion to less than 15%. The reactant mixture for TOF measurements consisted of 0.8% C_3H_8 and 9.9% O_2 with Ar as a diluent. Carbon dioxide and water were the only products formed. The carbon balance closed within 5%. Stability of the 1cPt/STO nanocuboid catalyst was also checked by holding the catalyst at these conditions for 65 h. Turnover frequency was calculated based on the moles of C_3H_8 consumed per total moles of platinum (TOF_t) and per moles of surface platinum (TOF_s), with the percentage of surface platinum coming from CO chemisorptions results. Lean conditions were used in all cases to obtain good propane kinetics.

3. RESULTS AND DISCUSSION

3.1. Pt Atomic Layer Deposition. Pt loading for 1, 3, and 5 cycles Pt/STO was 4.7, 9.7 and 15.2 wt % Pt, respectively. Pt loading increased by 4.7 wt % for the first cycle, and only by 2.6 wt % on average for cycles 2 through 5. Using the STO surface area of 20 m^2/g and the previously observed Pt ALD growth rate of 0.5 Å per cycle,[43] the expected mass gain is 2.1 wt % per cycle. It has been previously observed that the Pt growth rate via ALD on STO prior to film closure is faster than after film closure.[46] Thus it is expected that the growth rate would be higher than 2.1 wt % as STO is exposed in all cases, and the highest for the initial cycle as in that case no STO was blocked by previous Pt deposition. The initial growth of ALD metals on oxide surfaces is typically of Volmer−Weber type and proceeds via the nucleation and growth of islands. Even though the platinum precursor prefers to adsorb on the oxide rather than the metal,[33] islands are thermodynamically favored,[32] and likely grow as the precursor ligands are burned off.

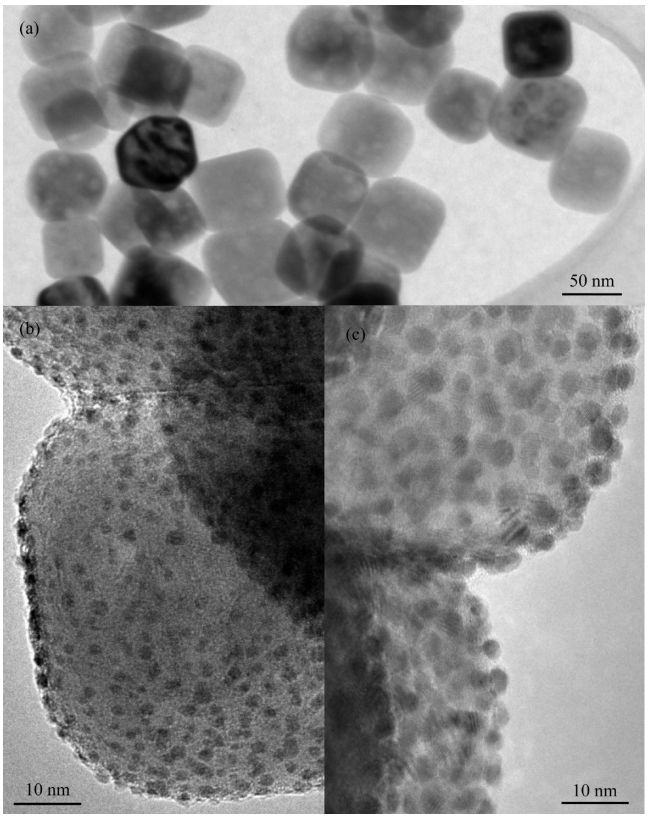

Figure 1. TEM images of $SrTiO_3$ nanocuboids (a) as prepared and following (b) 1 and (c) 5 cycles Pt ALD.

3.2. Pt Nanoparticle Morphology. The morphology of STO nanocuboids has been described in detail elsewhere.[41] Briefly, these are nonporous, single-crystalline, cubic-shaped particles, with an average edge length of 60 nm (Figure 1a), and a BET surface area of 20 m^2/g.

SEM (not shown) and TEM imaging (Figure 1) of the Pt coated STO nanocuboids shows that the ALD Pt deposited as small, well dispersed nanoparticles. SEM imaging of the 1c Pt on STO powder (not shown) revealed small, well dispersed nanoparticles similar to the 1c Pt on STO nanocuboids (Figure 1b). TEM and HREM imaging were employed to further assess the size distribution, dispersion, and crystallinity of Pt nanoparticles deposited after 5 ALD cycles, both before and after catalytic testing. As-deposited Pt nanoparticles exhibit very narrow size distribution, with sizes ranging from 1 to 5 nm, depending upon number of ALD cycles, and remarkable uniform dispersion over the surface of the oxide support; no significant agglomeration of

dx.doi.org/10.1021/cs200092c |ACS Catal. 2011, 1, 629–635

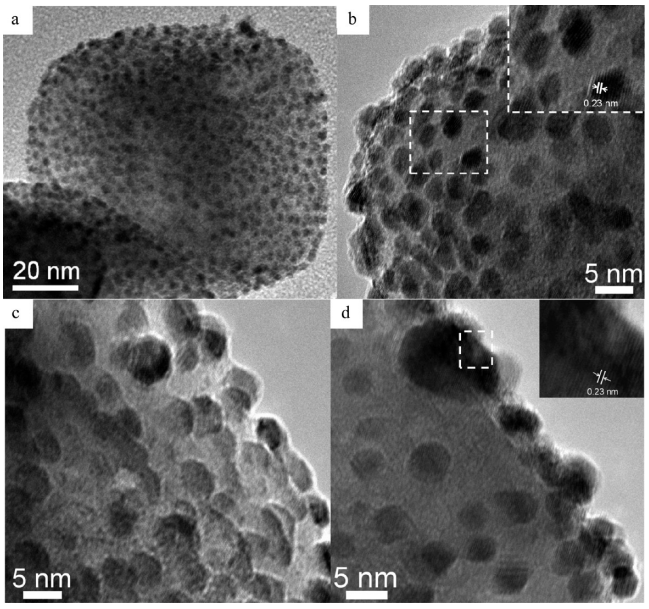

Figure 2. TEM pictures of 5 ALD cycles Pt/$SrTiO_3$. Top panel, before catalytic testing: (a) a single Pt/$SrTiO_3$ nanocuboid; (b) corresponding near cube-edge image (Inset: HREM image of Pt nanoparticles, showing lattice fringes corresponding to the [111] planes of Pt^0); Bottom panel, after 2 catalytic cycles from 25 to 500 °C: (c) and (d) near cube-edge images of two different Pt/$SrTiO_3$ nanocuboids.

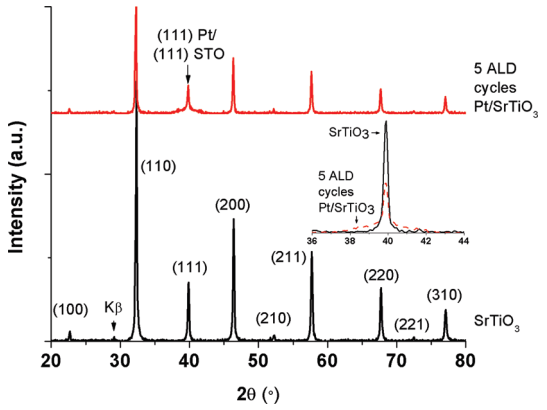

Figure 3. Powder X-ray diffraction patterns of as-prepared $SrTiO_3$ nanocuboids and 5 ALD cycles Pt/$SrTiO_3$. Inset: broadening of the (111) reflection of the perovskite phase because of overlap with the (111) reflection of Pt^0.

the metal particles was observed (Figure 2a–b). One Pt ALD cycle (TEM not shown) led to particles of 1–2 nm diameter, while five Pt ALD cycles (Figure 2a–b) produced platinum particles of 3–4 nm diameter. The dispersion estimated from CO chemisorption decreased from 75% for 1 cycle ALD to 35% for 5 cycles ALD, indicating particle sizes of 1.7 and 3.6 nm diameter, respectively. These sizes are consistent with literature reports of platinum particles prepared by ALD onto STO nanocuboids.[33,37] As expected, the lattice fringes match those of metallic Pt (PDF No. 04-0802, space group $Fm\bar{3}m$, $a \approx 3.92$ Å), and are consistent with the previously reported cube-on-cube epitaxy.[32] Powder X-ray diffraction analysis of the uncoated STO sample yielded a diffraction pattern (Figure 3) that can be indexed to the cubic space group $Pm\bar{3}m$ with lattice constant $a \approx 3.90$ Å

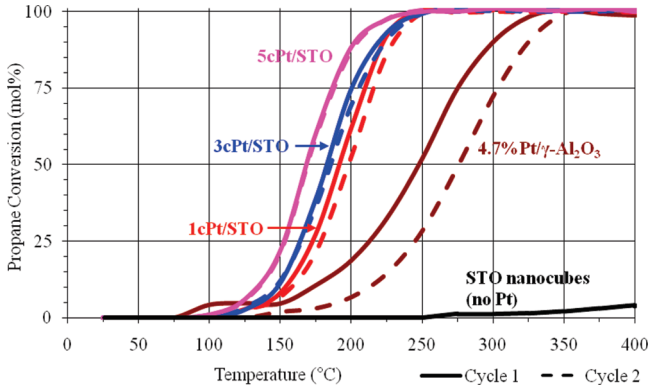

Figure 4. Propane oxidation light-off curves for 2 temperature cycles (25–400 °C) of 1c, 3c, and 5c Pt/$SrTiO_3$, 4.7% Pt/γ-Al_2O_3, and platinum-free STO nanocuboids with C_3H_8/O_2 = 1:16 and C_3H_8 WHSV = 4 h^{-1}. Solid lines for first temperature cycle, dashed lines for second temperature cycle.

(PDF No. 84-0444). For the 5cPt/STO sample, the broadening of the (111) peak of the perovskite phase, which is clearly evident, is due to overlap with the (111) reflection of Pt^0 (Figure 3), further supporting the presence of metallic platinum and epitaxy between STO and Pt. BET surface area measurement yielded a value of 31 m^2/g, indicating an increase of about 55% in surface area upon deposition of platinum.

TEM and HREM images of the sample after catalytic testing are shown in Figure 2c–d. Even though no chemical changes are apparent in HREM, that is, a large fraction of the Pt in the individual nanoparticles remains in its elemental form, the structural integrity of the metal nanoparticles deserves careful consideration. TEM imaging shows that although most areas of the oxide support remain homogeneously covered by Pt particles, the particles have grown slightly from ~3–4 nm to ~4–5 nm in average size (Figure 2c). Some other areas show less uniformly dispersed Pt particles with a broader size distribution (Figure 2d), indicating that they have undergone a sintering process.

3.3. Propane Oxidation Light-Off Temperature and TOF.

Figure 4 illustrates the propane oxidation light-off curves for 1cPt/STO, 3cPt/STO, and 5cPt/STO. For comparison, light-off curves of 4.7%Pt/γ-Al_2O_3 and of STO nanocuboids without any platinum are included. Light-off curves for both temperature cycles are identical for the Pt/STO nanocuboid samples. Over several temperature cycles, Pt particles may have minor sintering as shown in Figure 2c and d for 5cPt/STO. However, there was no detectable deactivation. Without Pt, STO was inactive for propane oxidation: during the light-off curve experiment, only 5% propane conversion was observed at the maximum temperature of 450 °C.

The light-off temperatures (T_{50}) and TOF are summarized in Table 1. WHSV were kept constant at 4 h^{-1} while determining the T_{50}. Thus, the total amounts of propane per total amount of Pt were equal in each experiment. For TOF measurement, WHSV were adjusted to achieve propane conversion of less than 10%. Propane T_{50} decreases from 198 to 168 °C, TOF_t at 250 °C increases from 368 to 7455 h^{-1} with increased Pt loadings, and TOF_s increases from 493 to 21162 h^{-1}. This trend could be the result of increasing Pt particle size for 1c-, 3c-, and 5cPt/STO.

Pt on STO nanocuboids shows great promise as a propane oxidation catalyst, superior to the conventional Pt/γ-Al_2O_3 catalyst. The two catalysts have comparable Pt loading, and the

dx.doi.org/10.1021/cs200092c |ACS Catal. 2011, 1, 629–635

Table 1. Propane Oxidation Turnover Frequency at 250°C and Light-Off Temperatures for Initial Cycle for Pt/$SrTiO_3$ Catalysts and Pt/Al_2O_3 Reference

catalyst	Pt weight %	support surface area (m^2/g)	Pt dispersion (%)[a]	est. particle size (nm)[a]	TOF_t (hr^{-1})[b]	TOF_s (hr^{-1})[b]	T_{50} (°C)[c]
1cPt/STO-N	4.7	20	75	1.7	368	493	192
3cPt/STO-N	9.7	20	67	1.9	1484	2201	183
5cPt/STO-N	15.2	20	35	3.6	7455	21162	168
1cPt/STO-S	0.4	2	69	1.8	16	23	
Pt/γ-Al_2O_3	4.7	175	48	2.6	6	13	247

[a] Pt dispersion and particle size estimated from CO chemisorption. [b] The space velocity was selected to maintain propane conversion lower than 10% on all samples. C_3H_8/O_2 = 1:13. [c] C_3H_8/O_2 = 1:16 and C_3H_8 WHSV = 4 h^{-1}.

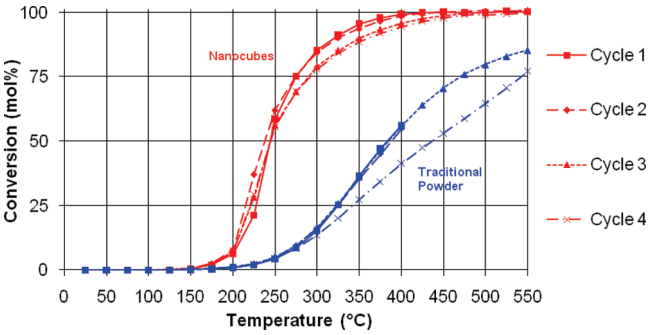

Figure 5. Propane oxidation light-off curves for 4 temperature cycles of 1cPt/STO nanocuboids and 1cPt/STO powder with C_3H_8/O_2 = 1:18 and C_3H_8 WHSV = 390 h^{-1}. Temperature range is 25−400 °C for the first two cycles on the powder support and 25−550 °C for cycles 3 and 4 on the powder support and for all four cycles on the nanocuboid support.

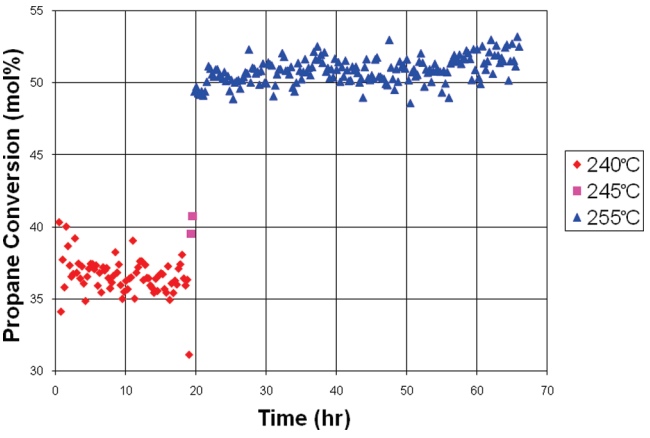

Figure 6. Activity of 1cPt/STO when run under catalytic conditions at ~250 °C for 65 at 380 h^{-1} WHSV and a 1:18 C_3H_8/O_2 ratio.

WHSV for light-off curve measurements were the same. 1cPt/STO T_{50} is approximately 75 °C less than T_{50} for 4.7%Pt/γ-Al_2O_3. Depending on the Pt loading, the propane TOF_t for Pt/STO is 60−1200 times higher than that measured for Pt/γ-Al_2O_3 in this study, 4−90 times higher than the Pt/γ-Al_2O_3 TOF reported by Garetto et al., and comparable to the Pt/zeolite results reported by Garetto et al.[47] Additionally, the Pt/STO nanocuboid catalyst shows greater resistance to deactivation. Whereas some deactivation was noted in the Pt/γ-Al_2O_3 catalyst after a single temperature cycle up to 400 °C (Figure 4), the Pt/STO nanocuboid catalyst showed minimal drop in activity or light-off temperature through four cycles up to 550 °C (Figure 5). Additionally, when running the Pt/STO nanocuboid catalyst at ~250 °C, no decrease in activity was observed over the course of nearly 3 days (Figure 6)

Figure 5 shows a comparison of 1cPt/STO on nanocuboid (4.7 wt %Pt) and a traditional solid state STO powder (0.4 wt %Pt) support. The WHSV was kept constant at 390 h^{-1} for both light-off temperature measurements. The activity of the Pt on STO nanocuboid supports is significantly greater than on conventional STO supports, and the light-off temperature was lower by more than 100 °C.

It has been proposed in the literature that the enhanced activity of the larger platinum particles is due to their remaining metallic, while the small platinum particles have lower activity because they become oxidized.[10−12] While there is evidence for correlation between activity and oxidation state, this particular theory of activity is unconvincing. First, metallic platinum cannot possibly function as an oxidizing agent, as there is no state more reduced than Pt^0 which the platinum could assume. Second, recent experimental results reveal that Pt particles on STO nanocube supports have similar oxidation behavior, regardless of size. EXAFS experiments have shown that in oxidizing environments Pt on STO nanocuboids has a PtO to Pt ratio that follows the platinum particle surface to volume ratio.[33,37] HREM investigations have confirmed that even the smallest platinum particles (1 cycle ALD) have a core of metallic platinum.[32] While the catalytic conditions used herein are not as strongly oxidizing as those used in previous EXAFS experiments, there is a significant excess of oxygen in the gas feed, making it likely that the surface will be oxidized. All Pt/STO nanocuboid catalysts are expected to have a similar Pt/PtO core/shell structure when subject to the same conditions. If such is the case, then it is likely that some other active phase exists, such as a single PtO monolayer over metallic platinum.

An alkane footprint size model has also been put forward to explain the increased activity of the larger platinum particles.[5] Platinum particles of smaller size would have far fewer faces of area large enough for an alkane molecule to bind than would larger platinum particles. However, it would be surprising if this alone accounted for the large observed difference in TOF (a factor of 20 for TOF_t and 87 for TOF_s) for an alkane as small as propane (<5 Å in length) when moving from 1 to 5 cycles ALD platinum particles.

The best working explanation may be a combination of the two, with both platinum particle size and oxidation state being relevant. If an oxidized monolayer over metallic Pt is formed, then the volume of the Pt core will be smaller than that of the particle overall. For a 1 nm platinum particle, there will only be a few metallic platinum atoms not bonded to oxygen either at the

dx.doi.org/10.1021/cs200092c |ACS Catal. 2011, 1, 629–635

Pt/STO interface or at the platinum particle surface. In such case a propane molecule would bind mostly to PtO_x over PtO_x or PtO_x over STO. For a 5 nm particle, there will be a ~4 nm metallic Pt core, and most propane molecules will bind to PtO_x over Pt. The oxidation of an alkane bonded to a monolayer of oxidized Pt over metallic Pt is consistent with current and previous observations. Similar concepts are known in other catalytic oxidation reactions. For example, oxidation of ethane over first row transition metal catalysts leaves the catalyst a mix of metal and metal oxide,[48] while using a catalyst initially prepared as a mixture of metal and metal oxide yields superior catalytic results.[49]

An active PtO_x over Pt catalyst also explains the STO nanocuboid supports having higher activity than either the solid state STO supports or the A_2O_3 supports. The Pt on the STO nanocuboid supports remains partly metallic platinum following treatment in 20% oxygen at 300 °C, whereas platinum on Al_2O_3 or TiO_2 supports Pt completely oxidized by the same treatment.[33] The metallic Pt is stabilized by the strong epitaxy with the STO nanocuboids.[32] Thermodynamically, the change in free energy for oxidizing the platinum particle would be the sum of the free energy for oxidizing the Pt ΔG^{PtO} and the difference in the energy terms associated with the interfacial free energy of Pt on the substrate γ_I^{Pt} and PtO γ_I^{PtO}. Approximating the particles as hemispheres (a more accurate model would use a Winterbottom construction[32]), we can write the effective free-energy change per unit volume for fully oxidizing a particle of radius R as

$$\Delta G^{Eff} = \Delta G^{PtO} + \frac{3(\gamma_I^{PtO} - \gamma_I^{Pt})}{2R}$$

For platinum metal upon STO (100) there is a strong epitaxy with γ_I^{Pt} quite negative due in part to the good match of lattice parameters. There is no obvious matching between PtO and STO (100). Hence the change in the interface free energy will make full oxidation less favorable, increasingly so as the size is reduced. Therefore the platinum at the interface (and because of strain energy terms, elsewhere as well) will not be oxidized for sufficiently small particles. For cases without a strong interface, such a barrier will be diminished, while in cases where the oxide has a strong interaction with the support (γ_I^{PtO} more negative) this will provide a driving force for complete oxidation. In such cases, larger platinum particles, with lower surface-to-volume ratios, would be required to stabilize a metallic platinum core. Conversely, stabilizing a metallic core at a smaller size through a large negative γ_I^{Pt} allows for active PtO_x/Pt core shell particles with higher surface-to-volume ratios.

The oxidized surface of the platinum particles is in a constant state of flux, being continuously oxidized by the oxygen, reduced by the propane, and reoxidized again by the oxygen. While kinetic parameters for O_2 adsorption on Pt are available, the lack of similar data for propane oxidation prevents the calculation of the equilibrium coverage of oxygen. Regardless, the stabilization of a metallic core by epitaxy with the support will prevent a stable, crystalline platinum oxide structure from forming. On supports where the entire particle is oxidized, the platinum oxide core will help stabilize the platinum oxide on the surface, thus making it less reactive. Similar effects have been found in other oxidation reactions over noble metal catalysts. For example, oxygen coverages on platinum of greater than one monolayer have been observed to lead to deactivation for NO oxidation by O_2 on Pt.[50] Significantly larger platinum particles may be necessary to prevent the complete oxidation of the platinum when using supports with a weaker epitaxy. During EXAFS studies in oxidizing conditions, all of the platinum on the Al_2O_3 supports was found to be oxidized.[33,37] Presumably the same occurs on powder STO supports as well. This is consistent with such supports exhibiting lower activity than the Pt/STO nanocuboid catalysts with even the smallest metallic Pt cores. Additionally, this is consistent with the report that platinum nanoclusters too small to possibly have a PtO_x over Pt structure lead to products other than total oxidation.[9]

In summary, Pt/STO nanocuboids exhibited lower T_{50} and higher TOF than either the standard Pt/Al_2O_3 or the Pt/STO powder. TEM images showed minor Pt ripening and sintering for 5cPt/STO after 2 temperature cycles up to 500 °C. The increased activity can be traced back to the strong epitaxy between the metallic platinum and the support which facilitates the creation of an active Pt/PtO core/shell structure during operating conditions. Pt/STO catalysts presented in this work contained Pt loadings over 4 wt %. These loading are higher than those used in commercial applications, for example, the typical three-way catalyst wash coat consists of only 1.1 wt % Pt.[51] However, because of the great increase in activity, the overall cost for the same activity may not be higher, and may even be lower, than commercial catalysts, and the high platinum loading should therefore not discourage further study.

4. CONCLUSIONS

Pt/STO shows promise as a highly active propane oxidation catalyst with a low propane light-off temperature and a high TOF. Pt nanoparticles deposited via ALD exhibit a narrow size distribution, with sizes ranging from 1 to 5 nm depending on the number of ALD cycles, and a remarkably uniform dispersion over the surface of the oxide support. Their structural integrity is minimally affected by catalytic testing because of ripening and interparticle sintering, and it does not appear to reduce the catalyst activity. The increased activity and stability can be attributed to the strong epitaxy between the nanocrystalline support and the platinum, which stabilizes platinum in the metallic phase. This leads to a Pt/PtO core shell type structure under oxidizing conditions, which is theorized to be the proximate cause of the increased activity.

AUTHOR INFORMATION

Corresponding Author

*Phone: 1-630-252-4310. Fax: 1-630-972-4408.

ACKNOWLEDGMENT

This work was supported by the U.S. Department of Energy, Office of Basic Energy Science, under Contracts W-31-109-ENG-38 and DE-FG02-03-ER15457 through the Institute for Catalysis in Energy Processes. The transmission electron imaging work was performed in the EPIC facility of NUANCE Center at Northwestern University. The NUANCE Center is supported by NSF-NSEC, NSF-MRSEC, Keck Foundation, the State of Illinois, and Northwestern University. SEM was performed at the Electron Microscopy Center for Materials Research at Argonne National Laboratory, a U.S. Department of Energy, Office of Science Laboratory operated under Contract No. DE-AC02-06CH11357 by UChicago Argonne, LLC.

REFERENCES

(1) Chang, C.; Lo, J.; Wang, J. *Atmos. Environ.* **2001**, *35*, 6201.
(2) Ristovski, Z. D.; Jayaratne, E. R.; Morawska, L.; Ayoko, G. A.; Lim, M. *Sci. Total Environ.* **2005**, *345*, 93.

(3) Tanaka, M.; Tsujimoto, Y.; Miyazaki, T.; Warashina, M.; Wakamatsu, S. *Chemosphere* **2001**, *3*, 185.
(4) Heck, R.; Farrauto, R. *Appl. Catal., A* **2001**, *221*, 443.
(5) Yao, Y. F. Y. *Ind. Eng. Chem. Prod. Res. Dev.* **1980**, *19*, 293.
(6) Briot, P.; Auroux, A.; Jones, D.; Primet, M. *Appl. Catal., A* **1990**, *59*, 141.
(7) Carballo, L.; Wolf, E. *J. Catal.* **1978**, *53*, 366.
(8) Lee, A.; Wilson, K.; Lambert, R.; Hubbard, C.; Hurley, R.; McCabe, R.; Gandhi, H. *J. Catal.* **1999**, *184*, 491.
(9) Vajda, S.; Pellin, M. J.; Greeley, J. P.; Marshall, C. L.; Curtiss, L. A.; Ballentine, G. A.; Elam, J. W.; Catillon-Mucherie, S.; Redfern, P. C.; Mehmood, F.; Zapol, P. *Nat. Mater.* **2009**, *8*, 213.
(10) Yoshida, H.; Yazawa, Y.; Hattori, T. *Catal. Today* **2003**, *87*, 19.
(11) Yazawa, Y.; Yoshida, H.; Hattori, T. *Appl. Catal., A* **2002**, *237*, 139.
(12) Yazawa, Y.; Yoshida, H.; Komai, S.; Hattori, T. *Appl. Catal., A* **2002**, *233*, 113.
(13) Yuyao, Y. *J. Catal.* **1975**, *36*, 266.
(14) Libby, W. F. *Science* **1971**, *171*, 499.
(15) Alifanti, M.; Kirchnerova, J.; Delmon, B.; Klvana, D. *Appl. Catal., A* **2004**, *262*, 167.
(16) Simonot, L.; Garin, F.; Maire, G. *Appl. Catal., B* **1997**, *11*, 167.
(17) Boreave, A.; Tan, H.; Roche, V.; Vernoux, P.; Deloume, J.-P. *Solid State Ionics* **2008**, *179*, 1071.
(18) Musialik-Piotrowska, A.; Landmesser, H. *Catal. Today* **2008**, *137*, 357.
(19) Civera, A.; Negro, G.; Specchia, S.; Saracco, G.; Specchia, V. *Catal. Today* **2005**, *100*, 275.
(20) Giebeler, L.; Kiessling, D.; Wendt, G. *Chem. Eng. Technol.* **2007**, *30*, 889.
(21) Deak, D. S. *Mater. Sci. Technol.* **2007**, *23*, 127, and references therein.
(22) Enterkin, J. A.; Subramanian, A. K.; Russell, B. C.; Castell, M. R.; Poeppelmeier, K. R.; Marks, L. D. *Nat. Mater.* **2010**, *9*, 245.
(23) Calderone, V. R.; Testino, A.; Buscaglia, M. T.; Bassoli, M.; Bottino, C.; Viviani, M.; Buscaglia, V.; Nanni, P. *Chem. Mater.* **2006**, *18*, 1627.
(24) Diazguemes, M. I.; Carreno, T. G.; Serna, C. J.; Palacios, J. M. *J. Mater. Sci.* **1989**, *24*, 1011.
(25) Kao, C. F.; Yang, W. D. *Ceram. Int.* **1996**, *22*, 57.
(26) Moon, J.; Kerchner, J. A.; Krarup, H.; Adair, J. H. *J. Mater. Res.* **1999**, *14*, 425.
(27) Zheng, H.; Liu, X. Q.; Meng, G. G.; Sorensen, O. T. *J. Mater. Sci.: Mater. Electron.* **2001**, *12*, 629.
(28) Lencka, M. M.; Riman, R. E. *Ferroelectrics* **1994**, *151*, 159.
(29) Ahmad, T.; Ganguli, A. K. *J. Am. Ceram. Soc.* **2006**, *89*, 1326.
(30) Herrig, H.; Hempelmann, R. *Mater. Lett.* **1996**, *27*, 287.
(31) Rabuffetti, F. A.; Kim, H. S.; Enterkin, J. A.; Wang, Y. M.; Lanier, C. H.; Marks, L. D.; Poeppelmeier, K. R.; Stair, P. C. *Chem. Mater.* **2008**, *20*, 5628.
(32) Enterkin, J. A.; Poeppelmeier, K. R.; Marks, L. D. *Nano Lett.* **2011**, *11*, 993.
(33) Setthapun, W.; Williams, W. D.; Kim, S. M.; Feng, H.; Elam, J. W.; Rabuffetti, F. A.; Poeppelmeier, K. R.; Stair, P. C.; Stach, E. A.; Ribeiro, F. H.; Miller, J. T.; Marshall, C. L. *J. Phys. Chem. C* **2010**, *114*, 9758.
(34) Stair, P. C. *J. Chem. Phys.* **2008**, *128*, 182507.
(35) Pisduangdaw, S.; Panpranot, J.; Methastidsook, C.; Chaisuk, C.; Faungnawakij, K.; Praserthdam, P.; Mekasuwandumrong, O. *Appl. Catal., A* **2009**, *370*, 1.
(36) Symalla, M. O.; Drochner, A.; Vogel, H.; Buchel, R.; Pratsinis, S. E.; Baiker, A. *Appl. Catal., B* **2009**, *89*, 41.
(37) Christensen, S. T.; Elam, J. W.; Rabuffetti, F. A.; Ma, Q.; Weigand, S. J.; Lee, B.; Seifert, S.; Stair, P. C.; Poeppelmeier, K. R.; Hersam, M. C.; Bedzyk, M. J. *Small* **2009**, *5*, 750.
(38) Christensen, S. T.; Feng, H.; Libera, J. L.; Guo, N.; Miller, J. T.; Stair, P. C.; Elam, J. W. *Nano Lett.* **2010**, *10*, 3047.
(39) Feng, H.; Elam, J. W.; Libera, J. A.; Setthapun, W.; Stair, P. C. *Chem. Mater.* **2010**, *22*, 3133.
(40) Elam, J. W.; Zinovev, A. V. V.; Pellin, M. J.; Comstock, D. J.; Hersam, M. C. *ECS Trans.* **2006**, *3*, 271.
(41) Rabuffetti, F. A.; Kim, H.-S.; Enterkin, J. A.; Wang, Y.; Lanier, C. H.; Marks, L. D.; Poeppelmeier, K. R.; Stair, P. C. *Chem. Mater.* **2008**, *20*, 5628.
(42) Libera, J. A.; Elam, J. W.; Pellin, M. J. *Thin Solid Films* **2008**, *516*, 6158.
(43) Aaltonen, T.; Ritala, M.; Sajavaara, T.; Keinonen, J.; Leskela, M. *Chem. Mater.* **2003**, *15*, 1924.
(44) Elam, J. W.; Groner, M. D.; George, S. M. *Rev. Sci. Instrum.* **2002**, *73*, 2981.
(45) Gluhoi, A. C.; Bogdanchikova, N.; Nieuwenhuys, B. E. *Catal. Today* **2006**, *113*, 178.
(46) Christensen, S. T.; Elam, J. W.; Lee, B.; Feng, Z.; Bedzyk, M. J.; Hersam, M. C. *Chem. Mater.* **2009**, *21*, 516.
(47) Garetto, T. F.; Rincon, E.; Apesteguia, C. R. *Appl. Catal., B* **2007**, *73*, 65.
(48) Lin, X. F.; Hoel, C. A.; Sachtler, W. M. H.; Poeppelmeier, K. R.; Weitz, E. *J. Catal.* **2009**, *265*, 54.
(49) Lin, X. F.; Poeppelmeier, K. R.; Weitz, E. *Appl. Catal., A* **2010**, *381*, 114.
(50) Smeltz, A. D.; Delgass, W. N.; Ribeiro, F. H. *Langmuir* **2010**, *26*, 16578.
(51) Bartholomew, C.; Farrauto, R. *Fundamentals of Industrial Catalytic Process*, 2nd ed.; John Wiley & Sons, Inc.: Hoboken, NJ, 2006.